

Well-constructed Ni@CN material derived from di-ligands Ni-MOF to catalyze mild hydrogenation of nitroarenes

Haijun Pan, Yuanyuan Peng, Xinhuan Lu*, Jie He, Lin He, Chenlong Wang, Fanfan Yue, Haifu Zhang, Dan Zhou, Qinghua Xia*

Hubei Collaborative Innovation Center for Advanced Organic Chemical Materials & Ministry-of-Education Key Laboratory for the Synthesis and Application of Organic Functional Molecules, Hubei University, Wuhan, 430062, PR China



ARTICLE INFO

Keywords:
Ni-MOFs
Ni@CN
Selective hydrogenation
Nitroarenes
Mild conditions

ABSTRACT

1,3,5-benzenetricarboxylate (BTC) and 4,4'-bipyridine (BIPY) are employed in the synthesis of dual ligands Ni-MOFs. The magnetic Ni@CN nanocatalyst is prepared by direct pyrolysis of Ni-MOFs in N₂ atmosphere, which exhibited excellent activity in selective hydrogenation of nitrobenzene (NB) to aniline (AN) at 60 °C, 2.0 MPa H₂. The conversion of NB can reach 99.1 mol%, and the selectivity of AN is over 99 %. A series of characterizations are obtained by XRD, Raman, XPS, SEM, TEM, TPR and TGA. It is found that the synergic effect of Ni species and N contributes to the increase of catalytic activity of the catalyst. Cycling tests proved that the prepared catalyst could be reused ten times without a visible reduction in catalytic activity of hydrogenation. The excellent stability and activity of Ni@CN nanocatalyst could be assigned to the porosity of carbon material doped with nitrogen, derived from dual ligands Ni-MOFs.

1. Introduction

It is a great challenge to pay attention to the environment and reduce the energy consumption and chemical waste in chemical transformation [1]. The selective hydrogenation of nitroarenes into corresponding anilines is widely used in the manufacture of various polymers, drugs, agricultural chemicals, dyes and pigments [2–4]. In the traditional industry, functionalized AN is mainly obtained by large amount of reducing agents such as sodium bisulfite, hydrazine hydrate or some non-recyclable non-noble metal ions (such as tin, iron, zinc), which will bring huge risks to the environment [5]. Therefore, there is an urgent need to develop an efficient and environmentally friendly way to produce AN. Catalytic hydrogenation with hydrogen as a hydrogen source is undoubtedly the best way to produce AN, owing to its low cost, cleanliness and ease of production. Nevertheless, in the past, most of the catalysts used in the catalytic hydrogenation reaction inevitably produced some by-products, such as azoxy derivatives, nitroso and hydroxylamines [6–8]. This is because the strong adsorption of intermediate products to catalysts increases the difficulty of selective hydrogenation of substituents on nitroarenes with other reducible groups (e.g., –OH, CC, CO, CN and C—=—=) [9–12].

Most of the literature on the production of aromatic amines is heavily dependent on precious metals, such as Pd, Pt, Rh, and Ru.

[1,13–16] The use of these precious metal catalysts can greatly increase the activity of the reaction, but the selectivity often does not perform well. Although selectivity can be improved by adding transition metal salts and additives to the reaction, the addition of these metal salts and additives poisons the reactive sites and reduces the reactivity, and the cost itself is high. Furthermore, it gives new problems to the environment [17,18]. Gold-silver based catalysts exhibit good selectivity for nitro compounds, but lower conversion due to its poor capacity of hydrogen dissociation [19,20]. With the increasingly strict environmental requirements in today's society, green chemistry is being called upon by more and more people, and heterogeneous catalysts for hydrogenation reactions play an important role in this process due to their easy separation characteristics. Therefore, there is an urgent need to develop a non-precious metal heterogeneous catalyst used for the hydrogenation of nitro compounds under mild conditions [21,22].

MOF is an inorganic-organic material composed of inorganic nodes and organic linkers [23–25]. Compared with traditional porous materials, MOFs have many characteristics such as high specific surface area, high porosity, and adjustable pore size [26,27]. Therefore, MOFs are often used in many fields such as catalysis [28–31], gas adsorption and separation [32,33], storage [34], fluorescence and molecular sensors [35–38]. Especially in the field of heterogeneous catalysis [39,40], MOFs materials and their derivatives are considered to be promising. At

* Corresponding authors.

E-mail addresses: xinhuan003@aliyun.com (X. Lu), xiqh518@aliyun.com (Q. Xia).

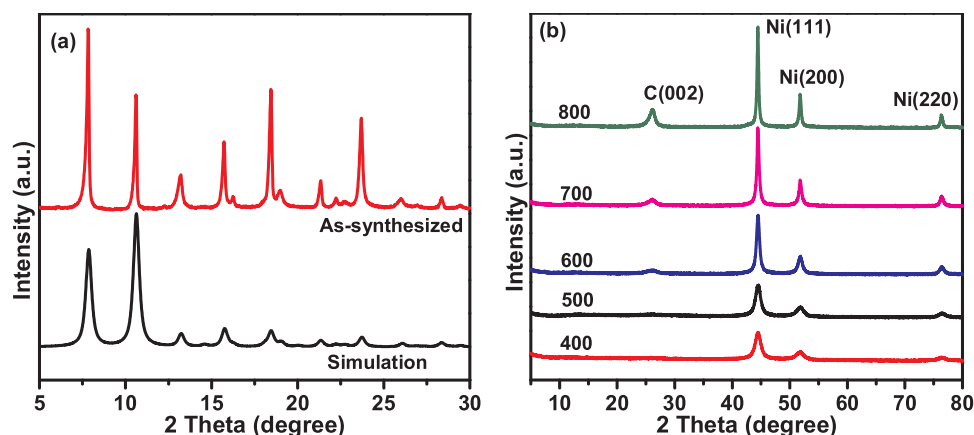


Fig. 1. Powder XRD patterns of (a) Ni-MOF precursor (b) Ni@CN-x materials prepared at various treatment temperatures.

present, the preparation of porous carbon-containing metals by means of pyrolysis of MOFs is a relatively simple method [41], and the application of the MOFs derivatives obtained after pyrolysis in hydrogenation reaction is also very common, e.g. in the hydrogenation of nitrobenzene to aniline [42–47].

Very recently, our group has published some works on the one step hydrogenation of NB [13,48], the hydrogenation product is cyclohexylamine. Herein, we report a simple preparation method for active N-doped Ni@CN catalyst and its applications in the selective catalytic hydrogenation of nitroarenes under mild conditions. The metal nanoparticles are uniformly distributed on the porous carbon, and the interaction between the nitrogen atoms and the nickel facilitates the formation of relatively electron-deficient and ultra-small sized nickel clusters.

2. Experimental

2.1. Materials

The chemicals used include $\text{Ni}(\text{NO}_3)_2 \cdot 6\text{H}_2\text{O}$ (98 %, Sinopharm), 1,3,5-benzenetricarboxylate (BTC, Aladdin), 4,4'-bipyridine (BIPY, Aladdin), DMF (98 %, Sinopharm), nitrobenzene (NB, 98 %, Sinopharm). All other chemicals are analyzed for purity.

2.2. Synthesis

2.2.1. Synthesis of Ni-MOF

Nickel nitrate hexahydrate ($\text{Ni}(\text{NO}_3)_2 \cdot 6\text{H}_2\text{O}$, 0.876 g, 3 mmol) as the metal source, BTC (2.270 g, 10.8 mmol) and BIPY (1.406 g, 9 mmol) as ligands, DMF as solvent are added in the PTFE liner. The ratio of metal to each ligand is (3 mmol: 10.8 mmol: 9 mmol = 1: 3.6: 3). When different ligand ratios are changed, other conditions such as temperature, time and synthesis method are remained the same. The mixture is stirred at room temperature for about 30 min and sealed into an autoclave, which is placed in an oven that has been preheated to certain temperature (60–150 °C) for some time (12–72 h). After the completion of crystallization, the content is cooled down to ambient temperature, recovered by filtration and washed with deionized water and DMF, followed by drying in 100 °C oven for 6 h to obtain green powder crystal, which is named as Ni-MOF precursor (a di-ligands Ni-MOFs material).

2.2.2. Preparation of Ni@CN-x catalysts

The precursor material obtained above is placed in a porcelain boat set in a vacuum tube furnace and pyrolyzed at 400–800 °C. Under the inert N_2 atmosphere, the furnace is heated to the targeted temperature with 2 h pyrolysis at 1 °C/min heating rate. After being cooled to room

temperature, a series of black solid powders are obtained and designated as Ni@CN-x (namely Ni@CN catalyst, where x represents the pyrolysis temperature).

2.3. Characterization of catalysts

Powder X-ray diffraction (XRD) is carried out on a Bruker D8A25 diffractometer operating under conditions of $\text{CuK}\alpha$ radiation (λ is 1.54184 Å) at 40 mA and 40 kV, ranging from 5 to 80° 2 θ . Raman spectra are obtained using a 512 nm argon ion laser (Renishaw Instruments, England) at a range of 100 to 4000 cm^{-1} . Scanning electron images (SEM) are recorded on a JEOL (JSM6700 F) with an accelerating voltage of 15 kV. Transmission electron microscopy (TEM) images are collected under JEOL-135 2010 F Transmission Electron Microscope at an accelerating voltage of 200 kV. X-ray photoelectron spectra (XPS) are collected on a Perkin-Elmer PHI ESCA system. Thermal gravimetric analysis (TGA) in N_2 atmosphere is performed on a PerkinElmer thermal analyzer. Temperature-programmed reduction using H_2 (H_2 -TPR) is carried out on the TP-5076 automatic gas sorption analyzer.

2.4. Selective hydrogenation

The catalytic reaction is carried out in a 25 ml stainless steel autoclave. Typically, (5.1–7.36 mol% [Ni]) of Ni@CN-x catalyst, 2 ml deionized water and 0.5 mmol nitrobenzene (NB) are added in sequence. After sealing the reactor, the air content is purged by flushing three times with 0.5 MPa H_2 . Then, the autoclave is heated to the given temperature at an agitation rate of 400 rpm. The temperature is monitored using a thermocouple inserted in the autoclave. The mixture in the system is diluted with ethanol, and the resulting reaction mixture is separated by centrifugation and analyzed by GC and GC–MS.

3. Results and discussion

3.1. Characterization of Ni@CN-x materials

Fig. 1(a) shows thus-synthesized Ni-MOF precursor and the simulated XRD patterns. The powder XRD pattern of the Ni-MOF matched well with the standard XRD pattern. The XRD patterns of Ni@CN-x catalysts obtained by calcining Ni-MOF precursor at different temperatures is shown in Fig. 1(b). The XRD patterns of the Ni@CN-x nanocatalysts exhibited three diffraction peaks at around 44.5°, 51.8° and 76.4°, corresponding to the characteristic diffractions of Ni [111], [200] and [220] lattice planes of metallic Ni, respectively (PDF# is 04-0850). The mean size of Ni NPs in Ni@CN-400, Ni@CN-500, Ni@CN-600, Ni@CN-700 and Ni@CN-800 is respectively calculated to be 8.0, 7.2,

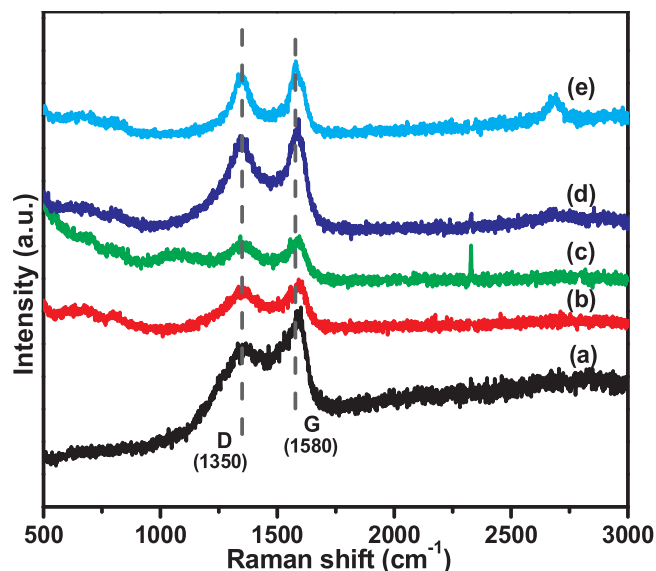


Fig. 2. Raman spectra of (a) Ni@CN-400, (b) Ni@CN-500, (c) Ni@CN-600, (d) Ni@CN-700 and (e) Ni@CN-800.

13.7, 20.4 and 27.0 nm according to the Scherer analysis based on the XRD results. The mean size of nanoparticles increases with an increase in the calcination temperature. When the calcination temperature is risen to 600, 700, and 800 °C, a new diffraction peak appears around 26.1°, attributed to the characteristic peak of graphite carbon.

Fig. 2 is the Raman spectra of Ni@CN prepared at different pyrolysis temperatures. The D band at $\sim 1350\text{ cm}^{-1}$ represents the disordered carbon with structural defects, while the G band at $\sim 1590\text{ cm}^{-1}$ represents the highly ordered graphitic carbon with sp^2 in-plane vibration. A higher I_D/I_G value indicates that the Ni@CN sample has more carbon matrix defects. The rise of the heating temperature from 400 to 500 °C leads to increase of I_D/I_G value from 0.804 to 1.071. The I_D/I_G value drops from 1.071 to 1.015 as the temperature is increased from 500 °C to 800 °C. This result indicates that there are more structural defects in the catalyst treated at 500 °C, confirmed by the catalyst activity in the hydrogenation of nitrobenzene.

The morphology of the dual ligands Ni-MOFs and Ni@CN-x catalysts are shown in Fig. 3. Fig. 3(a) shows that the morphology of Ni-

MOF is a regular hexagonal structure. It can be seen from Fig. 3(b) and (c) that as the pyrolysis temperature rises, the surface of the material begins to become rough, meaning that the active sites are slowly exposed. However, when the temperature exceeds 500 °C, the shrinkage and collapse of the surface of the material occurs clearly. By the pyrolysis temperature rising to 800 °C, the surface agglomeration of the material occurred severely. As the temperature increases, the Ni-MOFs precursor begins to transform to Ni@CN composite.

The morphology images of the Ni@CN-x catalyst is detected by TEM (Fig. 4, Table 1). It can be seen that the morphology of Ni-MOF is a hexagonal block structure. Its side length is about 4 μm and the thickness is about 0.6 μm . It is found that the Ni@CN-400 nickel nanoparticles are well distributed with small particle size. As shown, during the pyrolysis process nickel nanoparticles and elongated carbon tubes are gradually formed in the Ni@CN-500 catalyst. When the temperature exceeds 600 °C, the nickel nanoparticles are clearly observed. The particle size ranges from 1 to 40 nm, which increases with the increase of pyrolysis temperature. According to statistic results, the average particle sizes of Ni@CN-400, Ni@CN-500, Ni@CN-600, Ni@CN-700 and Ni@CN-800 are 8.6, 10.1, 15.7, 17.3 and 36.9 nm, respectively, consistent with XRD results. TEM images show that carbon nanotubes are formed at 500, 600, and 700 °C, but the pyrolysis temperature at 800 °C will cause the carbon nanotubes aggregated. At the same time, it can be clearly see from Fig. S1 that when the pyrolysis temperature is 800 °C, the material shows a very obvious core-shell structure and the active metal Ni is surrounded by a thick carbon shell.

Further XPS measurements of Ni@CN-400, Ni@CN-500, Ni@CN-700 and Ni@CN-800 are shown in Fig. 5. When the temperature ranges from 500 to 800 °C, significant binding energy transfer occurs in Ni 2p spectra of Ni@CN-x, which means that Ni species in Ni-MOF may be reduced to metal Ni particles in situ during thermal decomposition (Table 1). For example, when the decomposition temperature is 400 °C, the content of NiO is 44.6 %; while the temperature continues to rise to 500, 700 or 800 °C, the content of Ni⁰ is increased to 54.5, 58.5 or 62.8 %, respectively. According to previous reports, if the reduction potential of metal ions is -0.27 eV or higher (for example, Cu^{2+} , Co^{2+} and Ni^{2+}), they are easily reduced to metal nanoparticles in situ through a pyrolysis process under an inert atmosphere. At the same time, the peaks in Fig. 5(c) at 398.9 eV, 400.4 eV and 401.4 eV are classified as pyridinic N, pyrrolic N and graphitic N [49,50]. In Ni@CN-400, pyridinic N and pyrrolic N account for 50.1 and 49.9 % in total N atoms. However, in Ni@CN-500, pyridinic N proportion is 67.3 % and the

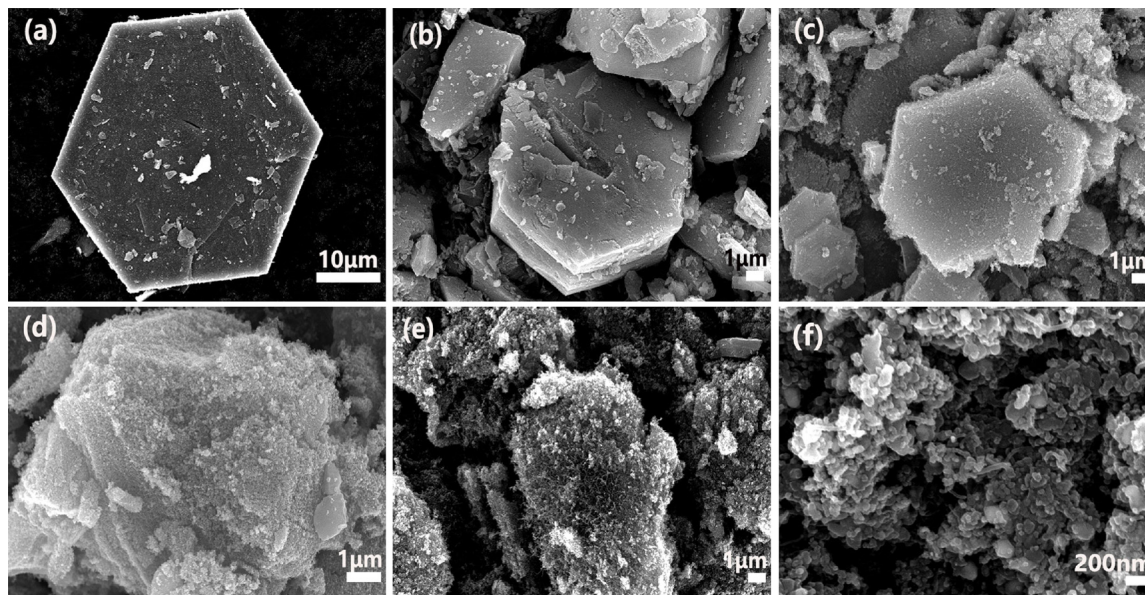


Fig. 3. SEM images of (a) Ni-MOF precursor, (b) Ni@CN-400, (c) Ni@CN-500, (d) Ni@CN-600, (e) Ni@CN-700 and (f) Ni@CN-800.

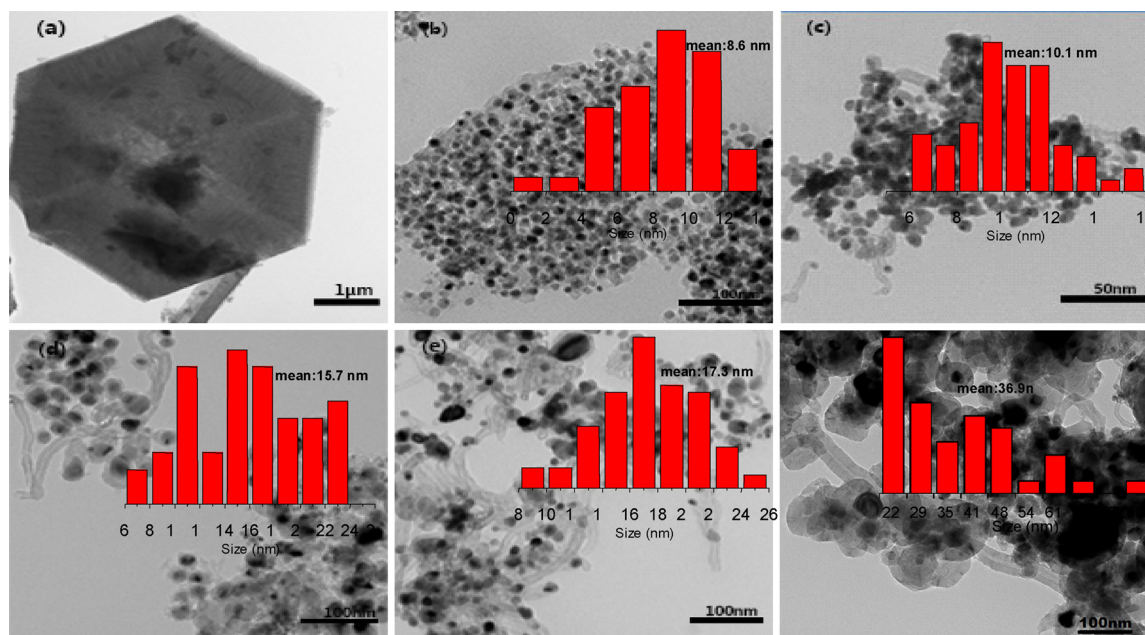


Fig. 4. TEM images of (a) Ni-MOF precursor, (b) Ni@CN-400, (c) Ni@CN-500, (d) Ni@CN-600, (e) Ni@CN-700 and (f) Ni@CN-800.

Table 1
Structural properties of Ni@CN-x.

Catalysts	Particle size (nm)		Relative atomic percentage (%) ^a			Relative atomic percentage (%)	
	XRD	TEM	N1	N2	N3	Ni ⁰	N ²⁺
Ni@CN-400	8.0	8.6	50.1	49.9	–	44.6	55.4
Ni@CN-500	7.2	10.1	67.3	32.7	–	54.5	45.5
Ni@CN-600	13.7	15.7	–	–	–	–	–
Ni@CN-700	22.4	17.3	46.4	21.3	32.3	58.5	41.5
Ni@CN-800	32.0	36.9	43.0	23.2	33.8	62.8	37.2

a: N1 — Pyridinic N, N2 — Pyrrolic N, N3 — Graphitic N.

pyrrolic N proportion is 32.7 % in total N atoms. Remarkably, as the temperature increases, graphitic N begins to appear. For example, when the pyrolysis temperature is 700 °C, graphitic N accounts for 32.3 %; at 800 °C graphitic N amount is increased to 33.8 %. This indicates that the transition metal can induce the generation of graphitic carbon at a high temperature. The C 1s peak of Ni@CN-x (Fig. 5d), located at approximately 284.5 eV with one tail peak at 288.4 eV, is assigned to C–Ni bonding and the electron-deficient carbons bound to nitrogen (C–N), respectively [51]. With increasing the pyrolysis temperature, this CN–signal is weakened significantly, suggesting that the pyridine-like or aromatic N is partly transformed into graphitic N in the carbon skeleton, this result is consistent with XRD and XPS characterization results. Too high temperature further weakens this signal. According to the analysis of ICP-AES, the metal Ni contents in Ni@CN-400, Ni@CN-500, Ni@CN-700 and Ni@CN-800 are 37.88, 39.89, 33.81 and 34.12 %, respectively.

As displayed in thermogravimetric analysis (TG) curves, both Ni-MOF and Ni@CN-x are stable up to 250 °C (Fig. 6). The weight loss at 30–250 °C is mainly due to the evaporation of the moisture and DMF molecules on the surface of the material. The weight loss at 250–470 °C is mainly attributed to the decomposition of BTC and BIBY, which indicates that the MOF skeleton has collapsed down. The weight loss at 470–660 °C is mainly due to the reduction of Ni species caused by pyrolysis, and further rise of the temperature does not result in an obvious weight loss. It is worthwhile mentioned that the weight loss rate of Ni@CN-500, Ni@CN-700 and Ni@CN-800 is slower than that of Ni@CN-400. This indicates that the increase of the pyrolysis

temperature may enhance the thermal stability of Ni@CN-x within a certain temperature range. The Ni@CN-500, Ni@CN-600, Ni@CN-800 have similar thermal stability, and the weight loss before 470 °C is attributed to the decomposition of DMF molecules and ligands. The weight loss after 470 °C is attributed to the pyrolysis of CHx. The specific loss amount corresponding to the temperature is shown in Table S1.

Fig. 7 presented that the H₂-TPR profiles of Ni@CN materials. In general, the interaction of metal species with carriers can create new surface compounds or alter their chemical states, further change reduction temperatures. The different reduction temperature regions represent the metal reducible ability or the strength of the metal-support interaction. As shown in the Fig. 7 that Ni@CN-400 has two signal peaks at 201 and 531 °C. The first peak is led by pyrolysis of the precursor into Ni⁰ particles, and the second signal peak indicates that Ni⁰ has a strong effect on the support. Ni@CN-500 has three signal peaks at 223, 348 and 568 °C, respectively. The front two signal peaks are led by the reduction of NiO particles to Ni⁰, while the signal peak at 568 °C indicates that Ni⁰ has strong interaction with the carrier. The three signal peaks on Ni@CN-700 have the same chemical behaviors as Ni@CN-500 at 199, 362 and 617 °C. The relatively weak peak on Ni@CN-800 indicates that the Ni sample is higher dispersion on the CN.

3.2. Catalytic performance

Fig. 8 shows the effect of different ligand ratios on catalyst hydrogenation (1: 3.6: 3.0 = Ni: BTC: BIPY). On condition that the total amount of the catalysts is kept the same in the NB hydrogenation reaction, the catalyst derived from the dual ligands Ni-MOF with appropriate ligands ratios show much higher NB conversion than ones from the single ligand Ni-BTC and Ni-BIPY. As-prepared Ni-BTC-500 pyrolyzed by Ni-BTC shows very low conversion of NB (52.6 %), indicating that Ni-BTC-500 derived from single ligand precursor is not an efficient catalyst for NB hydrogenation. This is due to the lack of the N element that can interact with the nickel nanoparticles to facilitate the reaction. Compared to Ni@CN-500 (di-ligands), Ni-BIPY-500 also exhibits a low activity in the NB hydrogenation (78.9 mol% of NB conversion). This may be due to the weak coordination ability between BIPY and Ni in the absence of BTC (low yield of Ni-BIPY), resulting in low catalytic activity. Combining the above two factors, we adopt the di-ligands

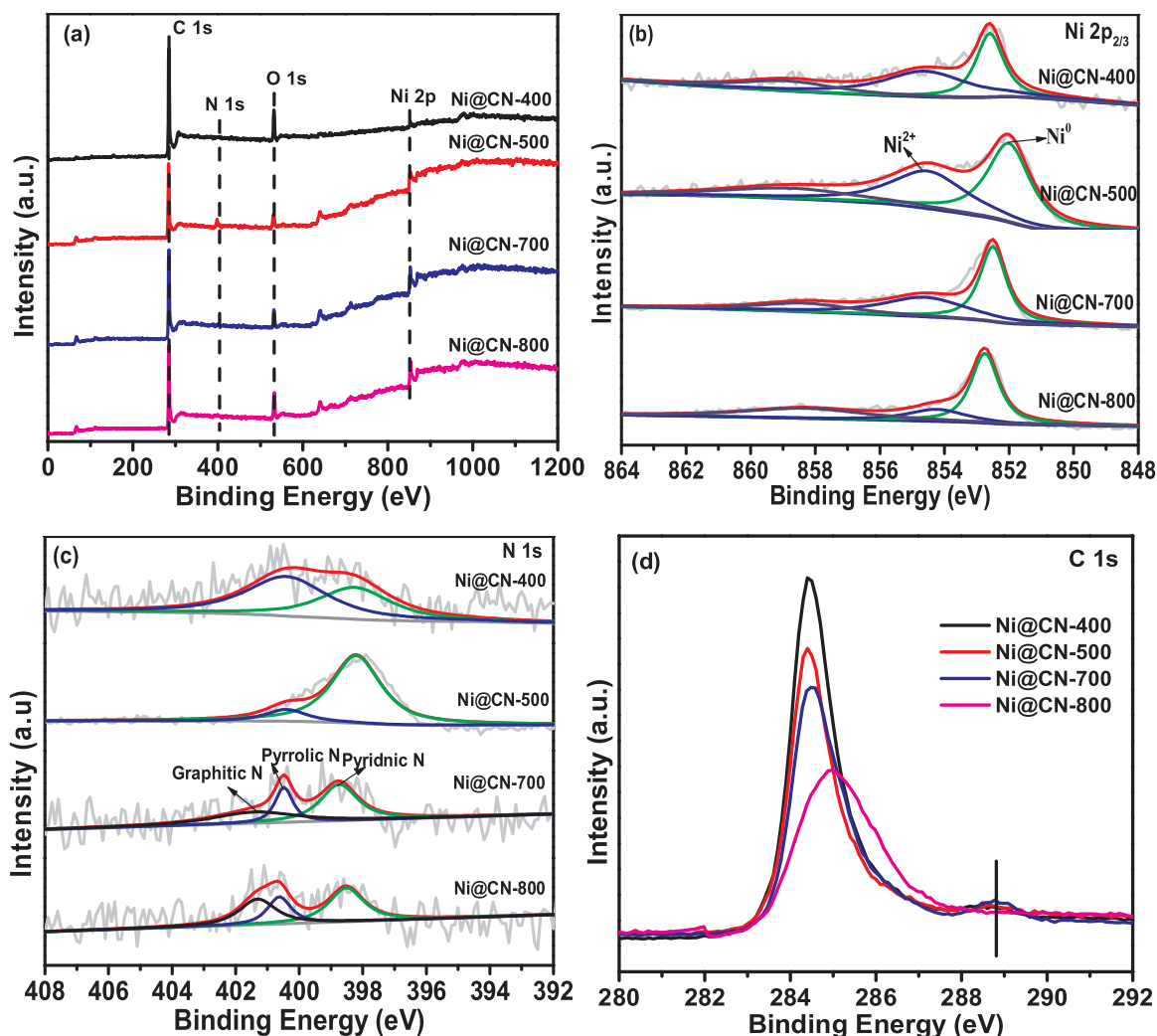


Fig. 5. XPS spectra of Ni@CN-x (a), Ni2p (b), N1 s (c) and C1 s (d).

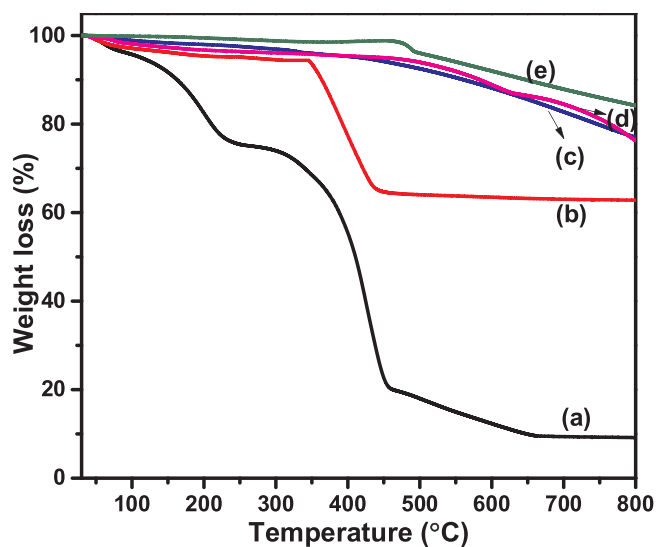


Fig. 6. TGA curves of (a) Ni-MOF precursor, (b) Ni@CN-400, (c) Ni@CN-500, (d) Ni@CN-700 and (e) Ni@CN-800.

strategy to overcome these two defects. The coordination capability of BIPY is enhanced and the N element is also introduced. Upon introducing the dual ligands into the precursor of Ni@CN-500, the

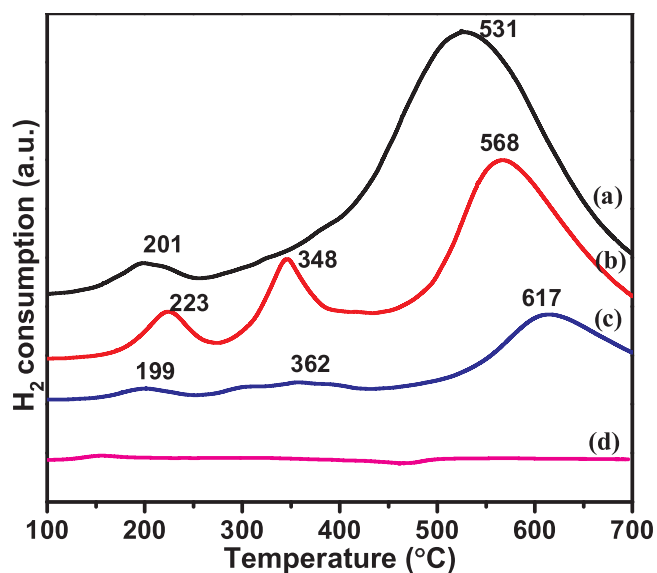


Fig. 7. H₂-TPR profiles of Ni@CN materials: (a) Ni@CN-400, (b) Ni@CN-500, (c) Ni@CN-700 and (d) Ni@CN-800.

activity of the resulting Ni@CN-500 increases much, appreciably higher than those of the mono-ligand led catalyst. Over the Ni@CN-500

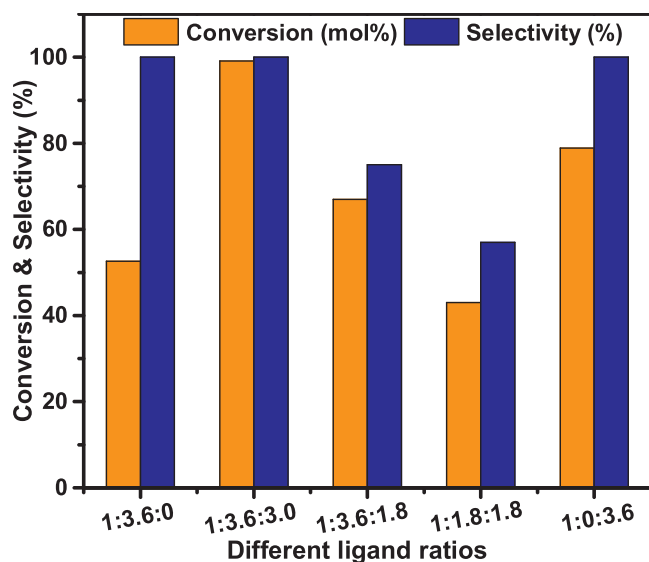


Fig. 8. Effect of different coordination ratios on catalyst performance in hydrogenation of NB (Reaction conditions: Ni@CN-500 catalyst (7.36 mol% [Ni]), 0.5 mmol NB, 2.0 ml H₂O, 60 °C, 2 h, 2.0 MPa H₂).

catalyst (the ratio of BTC: BIPY is 3.6:3.0), 99.1 mol% of NB conversion is achieved, which is the highest activity. However, with the decrease in the ratio of BTC: BIPY, NB conversions are obviously declined to 67.0 and 43.1 % (based on the ratio of BTC: BIPY is 3.6:1.8 or 1.8:1.8), respectively. In terms of the selectivity, the ratio of BTC: BIPY = 3.6:3.0 is the optimal beneficial to the formation of AN (> 99 % selectivity). Whereas the decrease in the ratio of BTC: BIPY to 3.6: 1.8 or 1.8: 1.8 will result in the decrease of cyclohexylamine selectivity. Therefore, the selection of the ligand ratio is very important. When the ratio of BIPY is small or the ratio of BTC and BIPY is reduced simultaneously, the conversion of the substrate and the selectivity of the product will be reduced. Moreover, the Ni@CN-x catalysts not only exhibits higher nitrobenzene conversion and selectivity for aniline, but also better catalytic activity under the conditions of H₂O as green reaction solvent, much low reaction temperature and low H₂ pressure than other Ni-based catalysts (Table S2) [13,42–45].

The effect of crystallization temperature and time on the catalytic hydrogenation of thus-prepared Ni@CN-500 in NB is presented in Fig. S2(a) and (b). The optimal crystallization temperature and time is 100 °C and 48 h. When the crystallization temperature is increased from 60 to 100 °C, the conversion of NB is increased from 9.7 to 99.1 mol%, and the selectivity of AN is increased from 75.3 to > 99 %. If the temperature is risen to 150 °C, the conversion of NB and the selectivity of AN are decreased to 15.6 mol% and 92.1 %. It is found that when the crystallization time of the precursor is 48 h, the conversion of NB is 99.1 mol%, with AN selectivity of > 99 %. As the crystallization time is risen from 12 to 48 h, the conversion of NB and the selectivity of AN are increased from 43.1 to 99.1 mol%, and from 84.8 to > 99 %. When the time is further increased to 72 h, the conversion of NB is decreased from 99.1 to 83.7 mol%, along with the decrease of AN selectivity from > 99 to 87.8 %.

Fig. 9 studies the effect of different pyrolysis temperatures on the hydrogenation of the catalyst. The blank reaction (without any catalyst) did not show any activity in this system. All the as-synthesized Ni@CN-x catalysts are highly active for this hydrogenation. It is quite clear that the catalysts prepared at suitable pyrolysis temperatures exhibit good catalytic activity. It can be seen that the Ni@CN-400 catalyst only gives 77.2 mol% conversion of NB with > 99 % selectivity to AN (Fig. 9), while Ni@CN-500 exhibits the highest conversion of 99.1 mol% and > 99 % selectivity to the target product AN. When the pyrolysis temperature is continuously risen from 500 to 800 °C, the conversion of

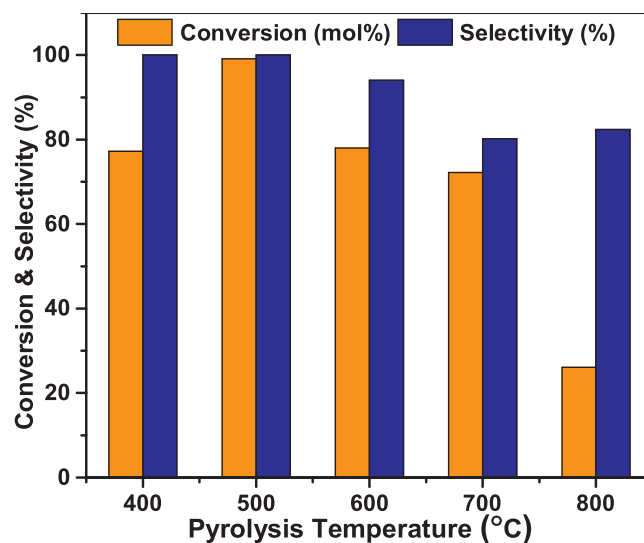


Fig. 9. The effect of pyrolysis temperatures on the catalytic performance of Ni@CN in NB hydrogenation (Reaction conditions: 5.1–7.36 mol% [Ni] catalyst, 0.5 mmol NB, 2.0 ml H₂O, 60 °C, 2 h, 2.0 MPa H₂).

NB is decreased from 99.1 to 26.1 mol%, and the selectivity of AN is decreased from > 99 to 82.4 %. These results indicate that the content and variation of N dopant has played important roles in the hydrogenation of NB (Fig. 5) As can be seen from Fig. 2, Ni@CN-500 has the highest I_D/I_G. And, Ni@CN-500 shows smaller particle size and more uniform distribution (Fig. 4). These characterizations can be combined to explain the good catalytic activity of Ni@CN-500. When the pyrolysis time of Ni@CN-500 is 2 h, the conversion of NB is 99.1 mol%, with AN selectivity of > 99 % (Fig. S3). With increasing the pyrolysis time from 1 to 2 h, the conversion is increased to 99.1 mol% in NB, and the selectivity of AN is lifted from 95.6 to > 99 %. As the pyrolysis time continues to increase (from 2 to 4 h), the conversion of NB is maintained at about 99.1 mol%, but the selectivity of AN is slightly decreased from > 99 to 97.4 %.

The influence of reaction temperature on catalytic activity is investigated under 30–80 °C at hydrogen pressure of 2.0 MPa, as shown in Fig. S4. At low hydrogen pressure of 2.0 MPa, even though the temperature raise is slightly varied from 30 to 60 °C, the AN yield is greatly increased from 13.3 % at 30 °C to 99.1 mol% at 60 °C, meaning significant effect of reaction temperature on reaction effect over Ni@CN-500 catalyst. When the reaction temperature is continuously increased from 60 °C to 80 °C, the conversion of NB is basically kept above 99 mol %. H₂ pressure has a large impact on catalytic activity (Fig. S5) and the observed conversion at 2.5 MPa (100 mol%) is more than 2.0 times higher than at 0.5 MPa (49.2 mol%). The selectivity towards AN also increases considerably from 85 % to > 99 % with increase of H₂ pressure from 0.5 to 2.0 MPa, respectively. Therefore, the hydrogenation of NB over Ni@CN-500 is more sensitive to H₂ pressure and reaction temperature.

Under the same conditions, we investigate the effect of solvent on the hydrogenation of NB (Fig. 10). The hydrogenation results show that the change in solvent significantly affects the reaction efficiency. Among the solvents tested, water is the optimal one, giving 99.1 mol% conversion of NB and > 99 % selectivity of AN. When the reaction solvent is ethyl acetate, the conversion of NB is 100 mol%, but the selectivity of AN is only 86.4 %. Toluene seems to be the worst one, which achieves the conversion of only 7.1 mol%, may be due to the low adsorption performance of the catalyst in toluene (Fig. 10). Obviously, the catalytic performance of NB hydrogenation reaction in polar solvents is much better than in non-polar solvents. The possible explanation could be that Ni@CN-500 catalyst with N doping usually possesses high hydrophilic properties, which results in homogeneous dispersion

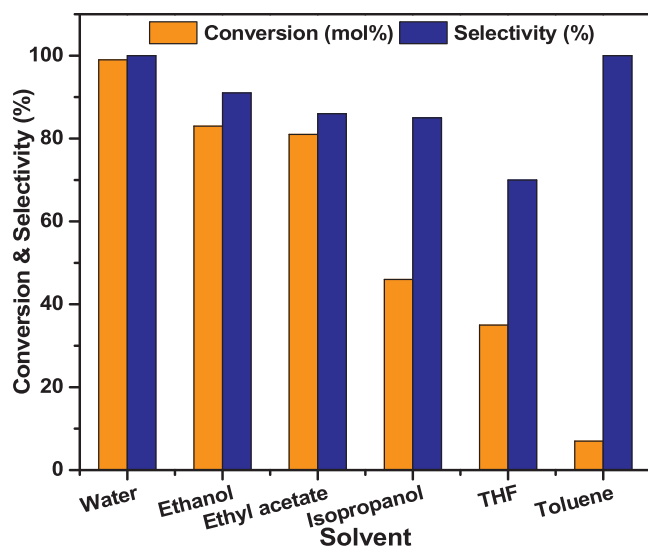


Fig. 10. Effect of reaction solvent on the hydrogenation of NB (Reaction conditions: Ni@CN-500 catalyst (7.36 mol% [Ni]), 0.5 mmol NB, 2.0 ml solvent, 60 °C, 2 h, 2.0 MPa H₂).

of the catalyst in water so as to improve the catalyst exposure to the reactants, consequently increasing the catalytic performance.

3.3. Stability and reusability of Ni@CN-500 catalyst

In terms of the reusability of the catalyst, we performed the selective hydrogenation of NB using Ni@CN-500 at 60 °C and 2.0 MPa in successive runs and compiled the results in Fig. 11. Due to the magnetic property of Ni-based material, it is easily separated from the solution using a magnet. The specific steps are as follows. After the reaction mixture is sampled, one magnet is placed at the bottom of the reactor until the catalyst is completely adsorbed to the bottom; when the solution becomes clear, a dropper is used to suck off the supernatant. The above steps are repeated, and the solid catalyst is washed three times with ethanol, followed by air-drying at room temperature. The recovered catalyst is applied in the next reaction under the same reaction conditions. Therefore, the stability and reusability of the Ni@CN-500 catalyst is proven in the hydrogenation of NB, in which the catalytic activity is maintained at almost a constant level. XRD patterns don't detect observable difference between fresh catalyst and 10 runs reused one (Fig. S6). The particle size distribution of the Ni@CN-500 after 10 cycles showed that the mean particle size is ~10.0 nm, almost the same with the fresh catalyst (Fig. S7).

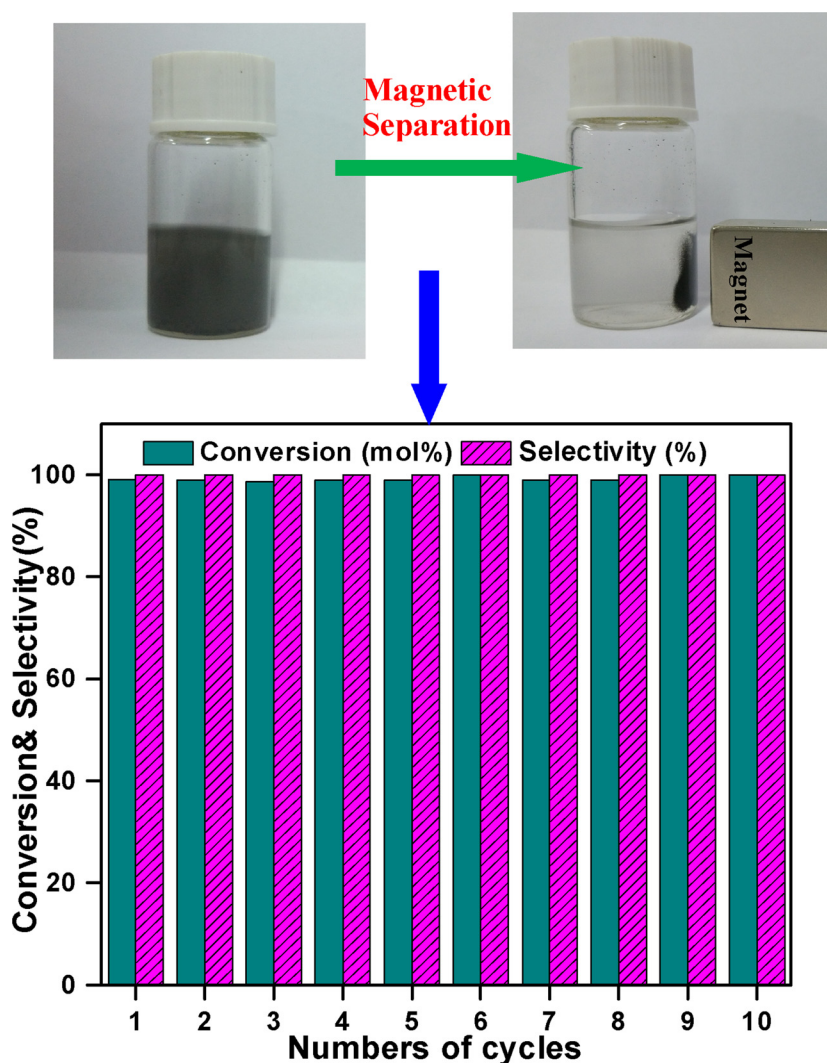
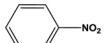
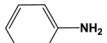
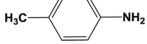
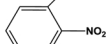
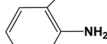
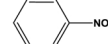
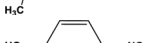
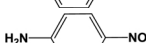
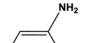
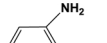
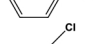
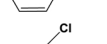
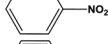
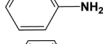
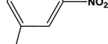
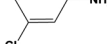
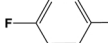
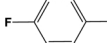
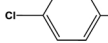
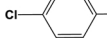
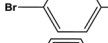
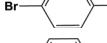
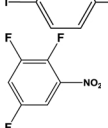
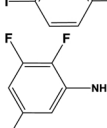
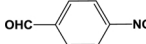
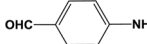
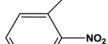
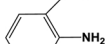


Fig. 11. Recycling tests of the catalyst Ni@CN-500 (Reaction conditions: 7.36 mol% [Ni] catalyst, 0.5 mmol NB, 2.0 ml H₂O, 60 °C, 2 h, 2.0 MPa H₂).

Table 2
Ni@CN-500-catalyzed hydrogenation of different substituted nitroarenes.

Entry	Substrate	Product	Reaction time (h)	Conversion (%)	Selectivity (%)
1			2	99.1	> 99
2			3	92.4	> 99
3			2	96.3	96.9
4			2	100	96.6
5			3	100	> 99
6			3	96.2	> 99
7			3	92.4	> 99
8			3	95.2	88.2
9			4	100	85.4
10			3	90.0	> 99
11			3	94.0	92.1
12			2	74.6	> 99
13			2	73.4	91.6
14			2	62.4	> 99
15			3	73.4	> 99
16			4	80.8	89.1

3.4. Chemoselective hydrogenation of various substituted nitroarenes

To explain the suitability of Ni@CN-500 catalysts better, we explore a series of other substituted nitroarenes. Expectedly, this catalyst has shown high conversion and selectivity for most nitroarenes. When the substituents on the aromatic ring of NB are methyl, hydroxy or amino group (Table 2, entry 2–7), the overall conversion efficiency is slightly better than that of halogenated nitroaromatics. This may be because these groups are electron-donating group, quite favorable for the selective hydrogenation on the benzene ring. Importantly, halogen-substituted nitrobenzenes can be reduced to halogenated anilines, known as an important agrochemical intermediate with high yield and no dehalogenation (entry 8–13). However, for multi-halogen substituted nitrobenzene like 2,3,5-trifluoronitrobenzene (entry 14), the reaction only can reach 62.4 mol% for 2 h. In addition, aldehydes as sensitive functional groups are well preserved in our catalytic systems (entry 15–16), among which nitrobenzaldehyde spends 4 h to obtain the conversion of only 80.8 mol%, with 89.1 % selectivity of *O*-aminoaldehyde.

Reaction conditions: 7.36 mol% [Ni] catalyst, 0.5 mmol substrate,

2.0 ml H₂O, 60 °C, 2.0 MPa H₂.

4. Conclusion

The dual-ligands Ni-MOF is synthesized by hydrothermal method, where BTC and BIBY provide carbon source and nitrogen source, which is then pyrolyzed under N₂ atmosphere to receive Ni@CN-*x* catalysts. The best crystallization and pyrolysis conditions are discussed, followed by a series of structural characterizations and catalytic tests. The effects of reaction solvent, temperature, time and H₂ pressure on the hydrogenation reaction are investigated systematically. In the hydrogenation of NB, the conversion of NB is up to 99.1 mol%, and the selectivity of AN is > 99 %. This high activity is due to the strong interaction between Ni nanoparticles and N species. Thus-prepared catalysts have excellent stability and recyclability.

Author contributions

All authors contributed to the writing of this manuscript and approved the final version of the manuscript.

Declaration of Competing Interest

The authors declare that they have no known competing financial interests or personal relationships that could have appeared to influence the work reported in this paper.

Acknowledgments

Financial support from the National Natural Science Foundation of China (21673069, 21503074, 21571055), Hubei Province Students Innovation and Entrepreneurship Training Foundation of China (201710512045), Hubei Province Outstanding Youth Foundation (2016CFA040), and Applied Basic Frontier Project of Wuhan Science and Technology Bureau (201911061251001).

Appendix A. Supplementary data

Supplementary material related to this article can be found, in the online version, at doi:<https://doi.org/10.1016/j.mcat.2020.110838>.

References

- S. Zhang, C. Chang, Z. Huang, J. Li, Z. Wu, Y. Ma, Z. Zhang, Y. Wang, Y. Qu, High catalytic activity and chemoselectivity of sub-nanometric Pd clusters on porous nanorods of CeO₂ for hydrogenation of nitroarenes, *J. Am. Chem. Soc.* 138 (2016) 2629–2637.
- H. Blaser, A golden boost to an old reaction, *Science* 313 (2006) 312.
- X. Meng, H. Cheng, Y. Akiyama, Y. Hao, W. Qiao, Y. Yu, F. Zhao, S. Fujita, M. Arai, Selective hydrogenation of nitrobenzene to aniline in dense phase carbon dioxide over Ni/γ-Al₂O₃: significance of molecular interactions, *J. Catal.* 264 (2009) 1–10.
- H. Wei, X. Liu, A. Wang, L. Zhang, B. Qiao, X. Yang, Y. Huang, S. Miao, J. Liu, T. Zhang, FeOx-supported platinum angle-atom and pseudo-single-atom catalysts for chemoselective hydrogenation of functionalized nitroarenes, *Nat. Commun.* 5 (2014) 5634.
- N. Daems, J. Wouters, C. Van Goethem, K. Baert, C. Poleunis, A. Delcorte, A. Hubin, I.F.J. Vankelecom, P.P. Pescarmona, Selective reduction of nitrobenzene to aniline over electrocatalysts based on nitrogen-doped carbons containing non-noble metals, *Appl. Catal. B* 226 (2018) 509–522.
- G. Vilé, N. Almora-Barrios, N. López, J. Pérez-Ramírez, Structure and reactivity of supported hybrid platinum nanoparticles for the flow hydrogenation of functionalized nitroaromatics, *ACS Catal.* 5 (2015) 3767–3778.
- D. He, X. Jiao, P. Jiang, J. Wang, B. Xu, An exceptionally active and selective Pt–Au/TiO₂ catalyst for hydrogenation of the nitro group in chloronitrobenzene, *Green Chem.* 14 (2012) 111–116.
- X. Liu, H. Li, S. Ye, Y. Liu, H. He, Y. Cao, Gold-catalyzed direct hydrogenative coupling of nitroarenes to synthesize aromatic azo compounds, *Angew. Chem. Int. Ed.* 53 (2014) 7624–7628.
- R. Millán, L. Liu, M. Boronat, A. Corma, A new molecular pathway allows the chemoselective reduction of nitroaromatics on non-noble metal catalysts, *J. Catal.* 364 (2018) 19–30.
- E.H. Boymans, P.T. Witte, D. Vogt, A study on the selective hydrogenation of nitroaromatics to N-arylhydroxylamines using a supported Pt nanoparticle catalyst, *Catal. Sci. Technol.* 5 (2015) 176–183.
- Z. Sun, Y. Zhao, Y. Xie, R. Tao, H. Zhang, G. Huang, Z. Liu, The solvent-free selective hydrogenation of nitrobenzene to aniline: an unexpected catalytic activity of ultrafine Pt Nanoparticles deposited on carbon nanotubes, *Green Chem.* 12 (2010) 1007–1011.
- W.C. Cheong, W.J. Yang, J. Zhang, Y. Li, D. Zhao, S.J. Liu, K.L. Wu, Q.G. Liu, C. Zhang, D.S. Wang, Q.P. Chen, Y.D. Li, Isolated iron single atomic site catalyzed chemoselective transfer hydrogenation of nitroarenes to arylamines, *ACS Appl. Mater. Interfaces* 11 (2019) 33819–33824.
- X. Lu, Y. Chen, Z. Zhao, H. Deng, D. Zhou, C. Wei, R. Nie, Q. Xia, Highly selective one-step hydrogenation of nitrobenzene to cyclohexylamine over the supported 10% Ni/carbon catalysts doped with 3% Rh, *RSC Adv.* 6 (2016) 15354–15361.
- W. Shi, B. Zhang, Y. Lin, Q. Wang, Q. Zhang, D.S. Su, Enhanced chemoselective hydrogenation through tuning the interaction between Pt nanoparticles and carbon supports: insights from identical location transmission electron microscopy and X-ray photoelectron spectroscopy, *ACS Catal.* 6 (2016) 7844–7854.
- S. Cai, H. Duan, H. Rong, D. Wang, L. Li, W. He, Y. Li, Highly active and selective catalysis of bimetallic Rh₃Ni₁ nanoparticles in the hydrogenation of nitroarenes, *ACS Catal.* 3 (2013) 608–612.
- Q. Yang, H. Zhang, L. Wang, Y. Zhang, J. Zhao, Ru/Uio-66 catalyst for the reduction of nitroarenes and tandem reaction of alcohol oxidation/knoevenagel condensation, *ACS Omega* 3 (2018) 4199–4212.
- A. Corma, P. Serna, P. Concepción, J.J. Calvino, Transforming nonselective into chemoselective metal catalysts for the hydrogenation of substituted nitroaromatics, *J. Am. Chem. Soc.* 130 (2008) 8748–8753.
- M. Makosch, W. Lin, V. Bumbálek, J. Sa, J.W. Medlin, K. Hungerbühler, J.A. van Bokhoven, Organic thiol modified Pt/TiO₂ catalysts to control chemoselective hydrogenation of substituted nitroarenes, *ACS Catal.* 2 (2012) 2079–2081.
- K. Shimizu, Y. Miyamoto, T. Kawasaki, T. Tanji, Y. Tai, A. Satsuma, Chemoselective hydrogenation of nitroaromatics by supported gold catalysts: mechanistic reasons of size- and support-dependent activity and selectivity, *J. Phys. Chem. C* 113 (2009) 17803–17810.
- K. Sun, Y. Hong, G. Zhang, B. Xu, Synergy between Pt and Au in Pt-on-Au nanostructures for chemoselective hydrogenation catalysis, *ACS Catal.* 1 (2011) 1336–1346.
- D. Formenti, F. Ferretti, F.K. Scharnagl, M. Beller, Reduction of nitro compounds using 3d-non-noble metal catalysts, *Chem. Rev.* 119 (2019) 2611–2680.
- R.V. Jagadeesh, A. Surkus, H. Junge, M. Pohl, J. Radnik, J. Rabeah, H. Huan, V. Schünemann, A. Brückner, M. Beller, Nanoscale Fe₂O₃-based catalysts for selective hydrogenation of nitroarenes to anilines, *Science* 342 (2013) 1073.
- A. Dhakshinamoorthy, M. Alvaro, H. García, Commercial metal–organic frameworks as heterogeneous catalysts, *Chem. Commun.* 48 (2012) 11275–11288.
- O.M. Yaghi, M. O’Keeffe, N.W. Ockwig, H.K. Chae, M. Eddaoudi, J. Kim, Reticular synthesis and the design of new materials, *Nature* 423 (2003) 705–714.
- A. Corma, H. García, F.X. Llabrés, I. Xamena, Engineering metal organic frameworks for heterogeneous catalysis, *Chem. Rev.* 110 (2010) 4606–4655.
- H. Deng, S. Grunder, K.E. Cordova, C. Valente, H. Furukawa, M. Hmadeh, F. Gandara, A.C. Whalley, Z. Liu, S. Asahina, H. Kazumori, M.O. Keeffe, O. Terasaki, J.F. Stoddart, O.M. Yaghi, Large-pore apertures in a series of metal-organic frameworks, *Science* 336 (2012) 1018.
- S. Dang, Q. Zhu, Q. Xu, Nanomaterials derived from metal–organic frameworks, *Nat. Rev. Mater.* 3 (2017) 17075.
- T. Sawano, P. Ji, A.R. McIsaac, Z. Lin, C.W. Abney, W. Lin, The first chiral diene-based metal–organic frameworks for highly enantioselective carbon–carbon bond formation reactions, *Chem. Sci.* 6 (2015) 7163–7168.
- K. Manna, T. Zhang, F.X. Greene, W. Lin, Bipyridine- and phenanthroline-based metal–organic frameworks for highly efficient and tandem catalytic organic transformations via directed C–H activation, *J. Am. Chem. Soc.* 137 (2015) 2665–2673.
- K.K. Tanabe, S.M. Cohen, Postsynthetic modification of metal–organic frameworks—a progress report, *Chem. Soc. Rev.* 40 (2011) 498–519.
- L. Jiao, Y. Wang, H. Jiang, Q. Xu, Metal–organic frameworks as platforms for catalytic applications, *Adv. Mater.* 30 (2018) 1703663.
- B. Li, H. Wen, Y. Cui, W. Zhou, G. Qian, B. Chen, Emerging multifunctional metal–organic framework materials, *Adv. Mater.* 28 (2016) 8819–8860.
- S. Xiang, Z. Zhang, C. Zhao, K. Hong, X. Zhao, D. Ding, M. Xie, C. Wu, M.C. Das, R. Gill, K.M. Thomas, B. Chen, Rationally tuned micropores within enantiopure metal–organic frameworks for highly selective separation of acetylene and ethylene, *Nat. Commun.* 2 (2011) 204.
- W. He, S. Li, W. Li, J. Li, G. Yang, S. Zhang, Y. Lan, P. Shen, Z. Su, Multipoint interactions enhanced H₂ storage and organosulfur removal in a microporous metal–organic framework, *J. Mater. Chem. A* 1 (2013) 11111–11116.
- N.B. Shustova, B.D. McCarthy, M. Dinca, Turn-on fluorescence in tetraphenylethylene-based metal–organic frameworks: an alternative to aggregation-induced emission, *J. Am. Chem. Soc.* 133 (2011) 20126–20129.
- H. Jiang, Y. Tatsu, Z. Lu, Q. Xu, Non-, micro-, and mesoporous metal–organic framework isomers: reversible transformation, fluorescence sensing, and large molecule separation, *J. Am. Chem. Soc.* 132 (2010) 5586–5587.
- B. Chen, S. Xiang, G. Qian, Metal–organic frameworks with functional pores for recognition of small molecules, *Acc. Chem. Res.* 43 (2010) 1115–1124.
- Y. Zhang, S. Yuan, G. Day, X. Wang, X. Yang, H. Zhou, Luminescent sensors based on metal-organic frameworks, *Coord. Chem. Rev.* 354 (2018) 28–45.
- T. Sawano, P. Ji, A.R. McIsaac, Z. Lin, C.W. Abney, W. Lin, The first chiral diene-based metal–organic frameworks for highly enantioselective carbon–carbon bond formation reactions, *Chem. Sci.* 6 (2015) 7163–7168.
- S. Rojas-Buzo, P. García-García, A. Corma, Catalytic transfer hydrogenation of biomass-derived carbonyls over hafnium-based metal–organic frameworks, *ChemSusChem* 11 (2018) 432–438.
- R. Das, P. Pachfule, R. Banerjee, P. Poddar, Metal and metal oxide nanoparticle synthesis from metal organic frameworks (MOFs): finding the border of metal and metal oxides, *Nanoscale* 4 (2012) 591–599.
- X. Wang, Y. Li, Chemoselective hydrogenation of functionalized nitroarenes using MOF-derived co-based catalysts, *J. Mol. Catal. A Chem.* 420 (2016) 56–65.
- A. Hu, X. Lu, D. Cai, H. Pan, R. Jing, Q. Xia, D. Zhou, Y. Xia, Selective hydrogenation of nitroarenes over MOF-derived Co@CN catalysts at mild conditions, *Mol. Catal.* 472 (2019) 27–36.
- P. Zhang, C. Yu, X. Fan, X. Wang, Z. Ling, Z. Wang, J. Qiu, Magnetically recoverable Ni/C catalysts with hierarchical structure and high-stability for selective hydrogenation of nitroarenes, *Phys. Chem. Chem. Phys.* 17 (2015) 145–150.
- W. Lin, H. Cheng, J. Ming, Y. Yu, F. Zhao, Deactivation of Ni/TiO₂ catalyst in the hydrogenation of nitrobenzene in water and improvement in its stability by coating a layer of hydrophobic carbon, *J. Catal.* 291 (2012) 149–154.
- Z. Liu, Y. Li, X. Huang, J. Zuo, Z. Qin, C. Xu, Preparation and characterization of Ni-B/SiO₂ sol amorphous catalyst and its catalytic activity for hydrogenation of nitrobenzene, *Catal. Commun.* 85 (2016) 17–21.
- Y. Qu, T. Chen, G. Wang, Hydrogenation of nitrobenzene catalyzed by Pd promoted Ni supported on C60 derivative, *Appl. Surf. Sci.* 465 (2019) 888–894.
- X. Lu, J. He, R. Jing, P. Tao, R. Nie, D. Zhou, Q. Xia, Microwave-activated Ni/carbon catalysts for highly selective hydrogenation of nitrobenzene to cyclohexylamine, *Sci. Rep.* 7 (2017) 2676.
- R. Nie, H. Yang, H. Zhang, X. Yu, X. Lu, D. Zhou, Q. Xia, Mild-temperature hydrodeoxygenation of vanillin over porous nitrogen-doped carbon black supported nickel nanoparticles, *Green Chem.* 19 (2017) 3126–3134.
- H. Yang, R. Nie, W. Xia, X. Yu, D. Jin, X. Lu, D. Zhou, Q. Xia, Co embedded within biomass-derived mesoporous N-doped carbon as an acid-resistant and chemoselective catalyst for transfer hydrodeoxygenation of biomass with formic acid, *Green Chem.* 19 (2017) 5714–5722.
- G. Deniau, L. Azoulay, P. Jégou, G. Le Chevallier, S. Palacin, Carbon-to-metal bonds: electrochemical reduction of 2-butenitrile, *Surf. Sci.* 600 (2006) 675–684.